Journal of Cluster Science (2022) 33:495–502
https://doi.org/10.1007/s10876-021-01994-w

ORIGINAL PAPER

Synthesis and Investigation of Template Effects on Nanoporous Bi_2O_3 Morphologies by Sol Gel Method as Photocatalysts for Degradation of Some Organic Dyes as Water Pollutants

Shanaz Arefi Moghadam[1] · Faezeh Farzaneh[1]

Received: 2 August 2020 / Accepted: 8 January 2021 / Published online: 23 January 2021

Abstract

Effect of triethanolamine, n-octylamine, starch, polyethylene glycol and hexadecyltrimethylammonium bromide as template have been investigated on the formation of Bi_2O_3 prepared via sol gel method. The prepared catalysts were characterized using X-ray diffraction, scanning electron microscopy, energy dispersive X-ray spectroscopy, Fourier transform infrared, UV–visible diffuse reflectance and Brunauer–Emmett–Teller techniques and subsequently used as photodegradation catalyst to purify contaminated water by Congo red and methylene blue as phenolic dyes. It was found that whereas $Bi_2O_{3\text{-starch}}$, $Bi_2O_{3\text{-CTAB}}$ and $Bi_2O_{3\text{-PEG}}$ have the most photodegradation effect on methylene blue under visible irradiation, $Bi_2O_{3\text{-starch}}$ and $Bi_2O_{3\text{-CTAB}}$ are the most active catalysts for Congo red under UV irradiation. In other word, the type of organic dyes, photocatalyst morphologies and templates are important factors on the photodegradation and adsorption phenomena.

Keywords Photodegradation · Bi_2O_3 · Template · Organic dyes

Introduction

In the past decades, many research works were focused on the metal and mixed metal oxides as photodegradation catalysts for organic dyes under visible or UV irradiation. Since synthesis of azo dyes as a class of colored organic compounds and their extensive application in several industries such as textiles, leathers, paper, and additives [1] contaminate water, a large quantity of waste water containing dyestuffs with intensive color and toxicity are introduced into the aquatic systems [2]. As such, removing of this contamination from waste water to less than 1 ppm is an important task since if not, it is clearly visible and influences the environment considerably [3]. Recall that whereas catalysts such as TiO_2, ZnO, Fe_2O_3, ZnS, WO_3, CdS and Bi_2O_3 have been used in this regard, amongst which bismuth oxide has many peculiar properties including significant band gap (from 2 to 3.96 eV), dielectric permittivity, high refractive index, and marked photoconductivity and photoluminescence [4, 5]. These properties have led to intense investigation of this material for applications in many areas such as microelectronics [6], sensor technology [7], optical coatings [8], and transparent ceramic glass manufacturing [9]. Since bulk Bi_2O_3 is a good optoelectronic material [10] with high photoconductivity [11], it is widely used in third order nonlinear optical glasses [12]. Bi_2O_3 is known with six polymorphic forms of monoclinic α-phase, tetragonal β-phase, body-centered cubic ϒ-phase, face centered cubic δ-phase, tetragonal ε-phase and triclinic ω-phase. Among these, whereas the α-phase and δ-phase are the most stable at room and high temperatures (730–825 °C) respectively, the other four are metastable phases [13]. It was found that photocatalysts with different crystal structures show quite different photocatalytic performances [14]. The previous study showed that α-Bi_2O_3, β-Bi_2O_3 and δ-Bi_2O_3 exhibit good photocatalytic activities in the degradation of pollutants [15]. Up

Supplementary Information The online version of this article (https://doi.org/10.1007/s10876-021-01994-w) contains supplementary material, which is available to authorized users.

✉ Faezeh Farzaneh
faezeh_farzaneh@yahoo.com; farzaneh@alzahra.ac.ir

[1] Department of Chemistry, Faculty of Physics and Chemistry, Alzahra of University, P.O. Box 1993891176, Vanak, Tehran, Iran

to now, α-Bi_2O_3 was mostly studied because of its thermal stability and easy preparation [16–19].

In this study, a number of Bi_2O_3 with different templates, morphologies and adsorptions were initially synthesized by sol–gel method and subsequently used as photodegradation catalyst to purify contaminated water by Congo red and methylene blue as phenolic dyes.

Experimental

Materials and Methods

Bismuth(III) nitrate pentahydrate $Bi(NO_3)_3{\cdot}5H_2O$, starch, polyethylene glycol (PEG), triethanolamine (TEA), n-octylamine (OA), hexadecyltrimethylammonium bromide (CTAB), nitric acid (HNO_3, 60%), NaOH (5N), HCl (5N), Congo red (CR) and methylene blue (MB) were purchased from Merck Chemical Company and used without further purification.

The prepared catalysts were characterized by X-Ray powder diffraction (XRD) from a KEFA Company, PW3050/60 (Theta/Theta) and with Cu-Kα radiation (λ = 0.154178 nm). Scanning electron microscopy (SEM) images were carried out on a Hitachi S-4800 microscope. UV–Vis diffuse-reflectance spectra were obtained with a Shimadzu-UV-2550-8030 with slit width 5.0 nm and light source change wavelength 360.0 nm spectrophotometer at room temperature. FT-IR spectra were obtained on a FT-IR spectrometer using Bruker, Tensor 27 DTGS, 500–4000 nm using KBr disks. Nitrogen adsorption–desorption measurements were obtained at 77 K with BELSORP Mini model from Microtrac Bel Corp, using Barrett–Emmett–Teller (BET) calculations for the surface area.

Synthesis of Photocatalysts

Synthesis of Bi_2O_3 Without Template

Bi_2O_3 was synthesized via the sol–gel method using $Bi(NO_3)_3{\cdot}5H_2O$ as precursor of Bi^{3+}. The synthesis procedure involved the homogenous dissolution of $Bi(NO_3)_3{\cdot}5H_2O$ (2 g, 4 mmol) in deionized water (20 mL) and HNO_3 (20 mL, 60%). The resultant mixture was kept under vigorous stirring at 90 °C until the solvent of the formed gel completely evaporated. The residue was then washed with ethanol to remove the impurities and dried at 80 °C for 24 h. The resultant solid was finally calcinated at 600 °C for 4 h.

Synthesis of Bi_2O_3 with TEA, OA, and Starch Templates

$Bi(NO_3)_3{\cdot}5H_2O$ (2 g, 4 mmol) was dissolved in deionized water (20 mL) and nitric acid solution (20 mL, 60%). After formation of a clear solution, the desired amount of templates such as TEA (1.1 mL, 8 mmol), OA (1.4 mL, 8 mmol), starch (1.33 g, 8 mmol) were added and the mixture stirred in 90 °C for 1 h on a water bath. The resultant mixtures were kept under vigorous stirring at 90 °C until the solvent of the formed gels completely evaporated. The residues were then washed with ethanol to remove the impurities and dried at 80 °C for 24 h. The resultant solids were finally calcinated at 600 °C for 4 h.

Synthesis of Bi_2O_3 with CTAB Template

$Bi(NO_3)_3{\cdot}5H_2O$ (2 g, 4 mmol) was dissolved in deionized water (20 mL) and nitric acid solution (20 mL, 60%). After formation of a clear solution, sodium hydroxide (3.5 mL, 5N) and CTAB (0.75 g, 2 mmol) were added and the mixture stirred in 90 °C for 1 h on a water bath. The resultant mixture was kept under vigorous stirring at 90 °C until the solvent of the formed gel completely evaporated. The residue was then washed with ethanol to remove the impurities and dried at 80 °C for 24 h. The resultant solid was finally calcinated at 600 °C for 4 h.

Synthesis of Bi_2O_3 with PEG Template

$Bi(NO_3)_3{\cdot}5H_2O$ (0.61 g, 1.2 mmol) was dissolved in deionized water (20 mL) and nitric acid solution (5 mL, 60%). After formation of a clear solution, distilled water (20 mL) and PEG (0.75 g, 2 mmol) were added and the mixture stirred in 90 °C for 1 h on a water bath. The resultant mixture was kept under vigorous stirring at 90 °C until the solvent of the formed gel completely evaporated. The residue was then washed with ethanol to remove the impurities and dried at 80 °C for 24 h. The resultant solid was finally calcinated at 600 °C for 4 h.

Catalytic Photodegradation of Organic Dyes

Photodegradations of Congo red and methylene blue as phenolic dyes were carried out under visible and ultraviolet light irradiations. As a general experiment, 0.05 g of the synthesized bismuth oxide either without or with template was poured into a crystallizer containing distilled water (100 mL) and dye (5 ppm). A 55 W UV or 60 W tungsten lamp was used as UV and visible light source respectively, using 8 cm distance between the incandescent light bulb and crystallizer. During the reaction, the air was always injecting into the solution through an oxygen pump to provide a constant amount of dissolved oxygen. Since

Congo red is anionic, the pH of the solution was initially adjusted to 3 with HCl (5N). Prior to irradiation, the complex was stirred in the dark for 15 min in order to become balanced for adsorption/desorption between the catalyst particles, dye and air oxygen. During irradiation, the solution color was sampled at specified intervals (every 15 min) and the catalyst was separated from the solution using centrifugation. The amount of degraded color was evaluated by measuring the rate of absorption changes by UV–Vis spectrophotometer.

Results and Discussion

To investigate the effect of different templates on Bi_2O_3 morphology, Bi_2O_3 with different templates such as TEA, starch, OA, CTAB and PEG was initially synthesized by sol–gel method (Scheme 1). In fact in this study attempts has been made to see the effect of different template on Bi_2O_3 morphology. Therefore the total procedure is the same but the type of template is different.

XRD Patterns

The XRD patterns of all calcined Bi_2O_3 associated with various templates such as TEA, OA, Starch, CTAB, and PEG shown in Fig. S1 (See Supplementary) are similar with the intensive and sharp peaks in the region of $2\theta = 27°$ and $2\theta = 33°$ related to the planes 120 and 200, respectively. These are consistent with the JCPDS card no. 2274-71 represent α-Bi_2O_3 with monoclinic crystalline phase [20].

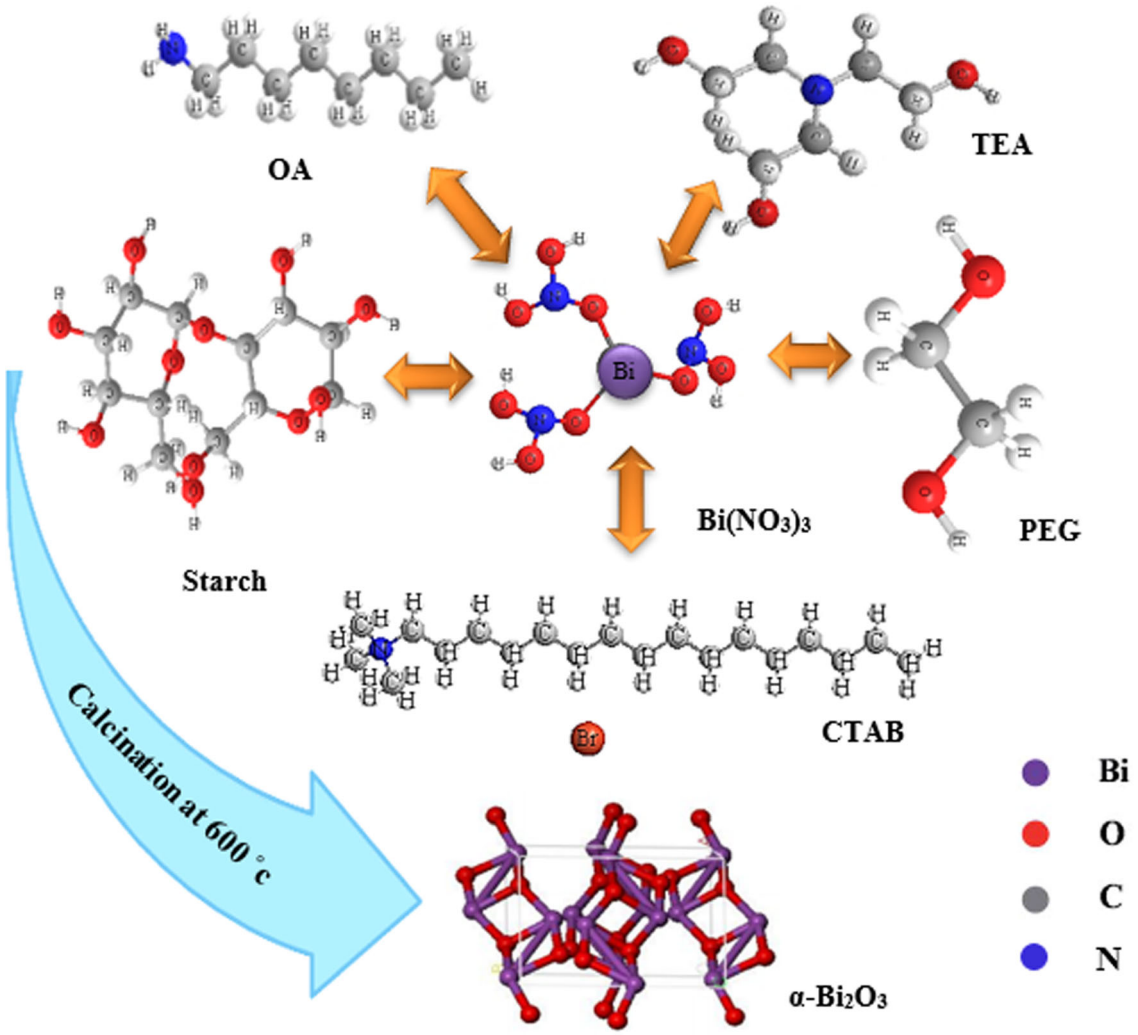

Scheme 1 Schematic of the synthesis of bismuth oxide catalysts with various morphologies

SEM Images

Based on the SEM image results, whereas the morphologies of $Bi_2O_{3\text{-}TEA}$ before calcination and Bi_2O_3 using no template have cubic and worm structures respectively (Fig. 1a, b), the former is transformed to the worm like morphology with 300–500 nm thickness after calcination (Fig. 1c, d). On the other hand, the morphology of the $Bi_2O_{3\text{-}OA}$ is porous with worm shape and diameter of about 250 nm with uniform surface and identical holes (Fig. 1e–f). Similarly, $Bi_2O_{3starch}$ is recognized with worm like morphology with cubic packing and the same size with a length of about 8 µm, consisting of particles with a diameter of about 500 nm and pore size of about 100–300 nm (Fig. 1 g, h). Finally, $Bi_2O_{3\text{-}CTAB}$ and $Bi_2O_{3\text{-}PEG}$ have morphologies of a bone structure with a diameter of about 1.5 to 2 µm with uniform surfaces (Fig. 2i–j) and porous cubic portions consisting of rods with diameter of about 500 nm with uniform distribution (Fig. 1k–l), respectively.

The results of the EDX analysis of bismuth oxide after calcination with different templates shown in Fig. S2a–f indicate the presence of bismuth, oxygen elements and trace amount of carbon.

The FTIR spectra of PEG, $Bi_2O_{3\text{-}PEG}$ hybrid before and after calcination at 600 °C and reusing as catalyst are shown in Fig. S3a–d, respectively. Whereas the peaks centered at 1705 and 1695 cm^{-1} are attributed to the R–O vibrations of PEG (see supplementary, Fig. 3Sa) [21], the two peaks observed at 1000 and 1320 cm^{-1} are due to R–O–R as ester groups. The appearance of two rather medium peaks at 400–700 and 1400 cm^{-1} after calcination are attributed to the Bi–O and Bi–O–Bi vibrations, respectively (Fig. 3Sc) [22, 23]. Particularly significant is the similarity observed in the FTIR spectra of Bi_2O_3 before and after using as catalyst (Fig. S3d). The remaining FTIR spectra of other templates are shown in the supplementary Figs. S4–8.

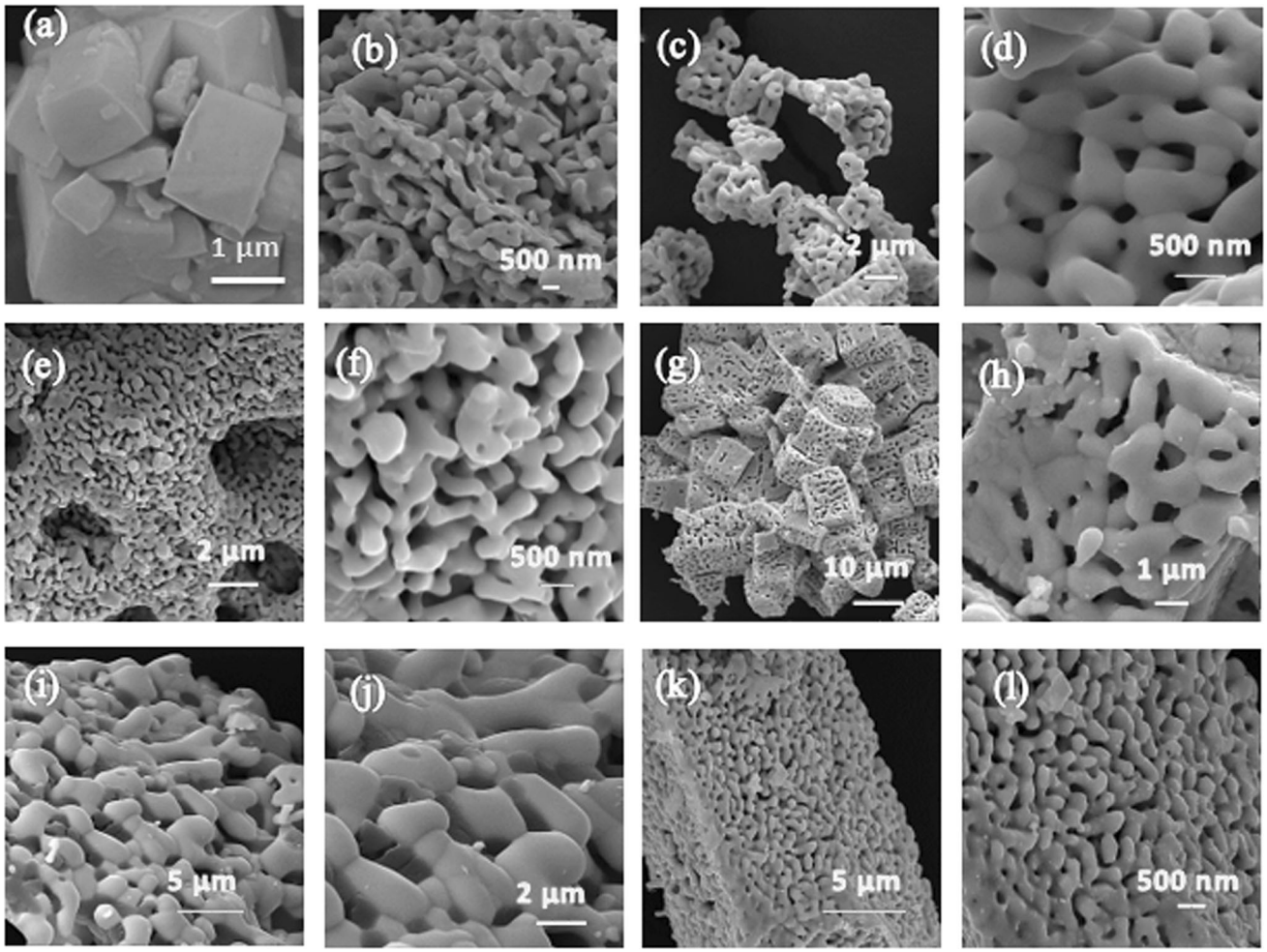

Fig. 1 The SEM images of the as-prepared Bi_2O_3 catalysts with various templates **a** hybride Bi_2O_3 and TEA template before calcined, **b** Bi_2O_3 with no template, **c**, **d** Bi_2O_3 with TEA template, **e**, **f** Bi_2O_3 with OA template, **g**, **h** Bi_2O_3 with starch template, **i**, **j** Bi_2O_3 with CTAB template, **k**, **l** Bi_2O_3 with PEG template

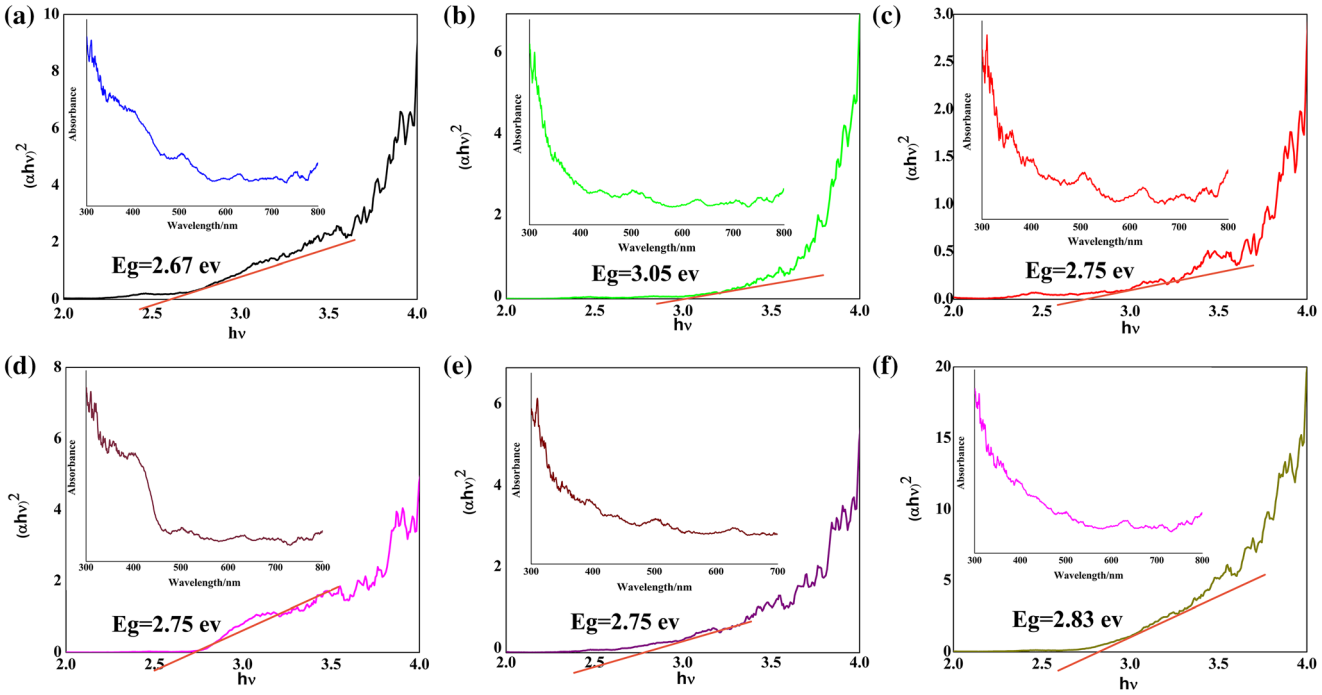

Fig. 2 The DRS analyze and band gap measurement of the as-prepared Bi_2O_3 catalysts with various templates, **a** Bi_2O_3 with no template, **b** Bi_2O_3 with TEA template, **c** Bi_2O_3 with OA template, **d** Bi_2O_3 with starch template, **e** Bi_2O_3 with CTAB template, **f** Bi_2O_3 with PEG template

The band gap, surface area and pore diameter of the prepared Bi_2O_3 with different morphologies are given in Table 1 and Fig. 2.

Photocatalytic Degradation of Bi_2O_3 with Different Morphologies

The results obtained for the degradation rate of CR and MB in the presence of Bi_2O_3 either without or with template as catalyst under visible and ultraviolet light irradiation are presented in Tables 2 and 3 and Fig. S9–12 (see supplementary). The model of kinetic destruction shown in Figs. S13 and S14 (see supplementary) are similar to that of Langmuir–Hinshelwood process (Eq. 1) [24]:

$$1/r = 1/k + 1/k\ K\ C \quad (1)$$

where r, k and K are reaction rate (mg/L min), limiting rate constant at maximum coverage under the given the experimental conditions and equilibrium constant for adsorption of the substrate, respectively. If the initial concentration C_0 is small, the Eq. 1 can be simplified to a first order equation which on integrating within the limits of concentration (C_0 to C) and time (0 to t) gives Eq. 2.

$$\mathrm{Ln}(C_0/C) = k\ K\ t = k_{app}t \quad (2)$$

Then, a plot of Ln (C_0/C) versus time gives a straight line with the slope of k_{app} and regression constant R_2 [25, 26] (Tables S2 and S3). Recall that the linear curves presented in Figs. S13 and S14 indicate that the photodegradation is approximately consistent with a first order kinetic, but for starch and cetyl shows some deviation from first order. This mechanism has also been used for the heterogeneous optical catalysts on the basis of cavity and electron production by optical excitation. The adsorbing color on the catalyst surface is degraded by the in situ generated active radical via the interaction with cavity. Subsequently, the catalyst is then re-produced.

Table 1 Some characteristics of prepared Bi_2O_3 with different templates

NUM	Catalyst	Band gap Eg (eV)	BET surface area as,BET	Mean pore diameter (nm)
1	No template	2.83	1.1108	14.064
2	Bi_2O_3- TEA	3.05	1.86491	9.3474
3	Bi_2O_3- OA	2.75	1.1238	15.362
4	Bi_2O_3- Starch	2.75	0.53468	18.451
5	Bi_2O_3- CTAB	2.75	0.51678	9.4091
6	Bi_2O_3- PEG	2.6	0.46201	7.6453

Table 2 Results of absorption and optical degradation tests against visible light and ultraviolet light for Congo red

Congo red				
NUM	Template name	%Absorption	%Degradation (Vis) After 30 min	%Degradation (UV) After 30 min
1	Without template	16.24	36.20	42.72
2	Triethanolamine	29.52	47.23	46.56
3	Octylamine	15.41	33.24	83.37
4	Starch	69.94	82.03	100
5	CTAB	50.74	55.98	100
6	Polyethylene glycol	3.23	3.23	78.97

Table 3 Results of absorption and optical degradation tests against visible light and ultraviolet light for methylene blue

Methylene blue				
NUM	Template name	%Absorption	%Degradation (Vis) After 30 min	%Degradation (UV) After 30 min
1	Without template	15.78	46.16	99.49
2	Triethanolamine	35.50	53.55	31.11
3	Octylamine	50.13	51	98.58
4	Starch	49.09	98.27	97.97
5	CTAB	91.64	99.34	98.85
6	Polyethylene glycol	7.52	94.10	96.70

A decrease in the intensity of the Congo red absorbance at 497, 347 and 235 nm is observed in the presence of bismuth oxide as catalyst on exposure of the solution to UV–visible light, perhaps due to the destruction of the azo chromophore band, naphthalene and benzoic rings, respectively. This may has occurred due to the direct or indirect oxidation through hydroxyl radicals generated by air oxygen and water present in the dye solution [27]. In methylene blue solution, the highest absorbance is observed in the 660 nm region. In the optical degradation of methylene blue, N-dealkylation of the alkylamine group exhibits the key feature of the photocatalytic degradation. The hypochromic shift occurs concurrently with the degradation of methyl groups [28, 29].

The photocatalytic properties of the prepared bismuth oxides as semiconductors were also investigated. As reported, the absorbing radiation is equal or higher than their energy band gap, metal oxide semiconductors can produce electrons in conduction band and holes in valence band, which have redox activities [30].

$$\text{Catalyst} + h\nu \rightarrow e_{cb}^{-} + h_{vb}^{+} \quad (3)$$

e_{cb}^{-} are electrons in the conduction band and h_{vb}^{+} is the cavities in the capacity layer respectively and can reduce the oxidation reactions with the catalysts. In most cases, h_{vb}^{+} reacts with H_2O attached to the catalyst surface and produces $OH^{\cdot}$ and e_{cb}^{-} reacts with O_2 to produce radical anion of oxygen superoxide.

$$H_2O + h_{vb}^{+} \rightarrow OH^{\cdot} + H^{+} \quad (4)$$

$$O_2 + e_{cb}^{-} \rightarrow O_2^{-\cdot} \quad (5)$$

These reactions will prevent the combination of cavities and electrons that created in the first phase. $OH^{\cdot}$ and O^{2-} can react with the colors and destroy them [31]. Dye is also converted to the cationic dye radicals ($Dye^{\cdot+}$) that undergoes degradation to yield products as given in Eqs. (6–8). The cationic dye radicals readily reacts with hydroxyl ions undergoing oxidation via Reactions 10 and 11 or interacts effectively with O_2^{-}, HO_2. or $HO^{\cdot-}$ species to generate intermediates that ultimately lead to CO_2 and H_2O [32, 33].

$$O_2^{-\cdot} + H_2O \rightarrow H_2O_2 \quad (6)$$

$$H_2O_2 \rightarrow 2\ OH^{\cdot} \quad (7)$$

$$OH^{\cdot} + \text{dye} \rightarrow \text{dye}_{ox} \quad (8)$$

$$\text{Dye} + e_{cb}^{-} \rightarrow \text{dye}_{red} \quad (9)$$

$$\text{Dye} + h_{VB}^{+} \rightarrow \text{dye}_{OX} \quad (10)$$

$$\text{Dye} + hv \rightarrow \text{Dye}^{\cdot+} \quad (11)$$

$$\text{Dye}^{\cdot+} + O_2^{-} \rightarrow DO_2 \rightarrow \text{degradation products} \quad (12)$$

$$\text{Dye}^{\cdot+} + HO_2^{\cdot}(\text{or } HO^{\cdot}) \rightarrow \text{degradation products} \quad (13)$$

Table 4 Photocatalytic activity of Bi_2O_3 in various structures or morphology

Entry	Morphology (Bi_2O_3)	Pollutants	Irradiation time	Photodegradation rate	Ref no.
1	Needles	MB	3 h	28%	[34]
2	Plates	MB	3 h	11%	[34]
3	Bounles of needles	MB	3 h	38%	[34]
4	Polyhedrons	MB	3 h	14%	[34]
5	α-Bi_2O_3	MB	6 h	30%	[35]
6	β- Bi_2O_3	MB	6 h	100%	[35]
7	Bi_2O_3	MB	9.5 h	16.7%	[36]
8	Bi_2O_3 (nanorods)	MB	1.5 h	65%	[37]
9	Bi_2O_3/CTAB	MB	0.5 h	99.34	Current work
10	Bi_2O_3/starch	MB	0.5 h[a]	99.27%	Current work
11	Bi_2O_3	CR[b]	1.5 h	62%	[38]
12	Bi_2O_3/starch	CR	0.5 h	82% 100%[c]	Current work

[a]*MB* methylene blue

[b]*CR* Congo red

[c]Under UV irradiation, the other reactions are under visible irradiation

The Effect of Photocatalyst Amount on Photodegradation of Organic Pollutants Dyes

The effect of photocatalyst amount on photodegradation rate of Congo red is shown in Fig. S15a, b (see supplementary). As seen, 0.09 g of catalyst for visible light and 0.05 g of catalyst under UV irradiation show 100% optical degradation of dye which represent the optimal amount of catalyst for purification of 100 mL color solution with 5 ppm concentration in 30 min.

The Effect of Bi_2O_3 Morphology as Catalyst on Photodegradation

Based on the obtained results, whereas $Bi_2O_{3Starch}$ is active for photodegradation of Congo red with 82% and 100% under Vis and UV irradiation, respectively (Table 2), $Bi_2O_{3Starch}$ or Bi_2O_{3CTAB} are the most active for photodegradation of methylene blue under visible irradiation (Table 3). On the other hand, it was found that Bi_2O_{3TEA} show the least catalytic activity for photodegredatoion of Congo red and methylene blue under Vis or UV irradiation (Tables 2, 3).

Finally, our results obtained for photocatalytic activity of Bi_2O_3 with various structures or morphologies has been compared with those of previously reported (Table 4) [34–37]. As seen in this Table, the effect of using metal free $Bi_2O_{3\text{-starch}}$ or $Bi_2O_{3\text{-CTAB}}$ and $Bi_2O_{3\text{-starch}}$ on the photocatalytic degradation of methylene blue and Congo red respectively under visible and visible or UV irradiations seem promising.

Conclusions

In conclusion, Bi_2O_3 with 5 different templates of TEA, OA, CTAB, Starch and PEG were prepared by sol gel method followed by calcination at 600 °C. The prepared samples were used as photodegradation catalyst for Congo red and methylene blue as organic colors under Vis and UV irradiation. It was found that whereas $Bi_2O_{3\text{-starch}}$, $Bi_2O_{3\text{-CTAB}}$ and $Bi_2O_{3\text{-PEG}}$ show the most photodegradation effect on methylene blue, $Bi_2O_{3\text{-starch}}$ and $Bi_2O_{3\text{-CTAB}}$ are the most active catalyst for photodegradation on Congo red under UV irradiation. In other word, the type of organic dyes, the morphology of photocatalysts and the templates are important factors on the photodegradation and adsorption phenomena.

Acknowledgements The financial support from Alzahra University is gratefully acknowledged.

Compliance with Ethical Standards

Conflict of interest The authors declare that they have no conflict of interest.

References

1. K. Kaur, R. Badru, P.-P. Singh, and S. Kaushal (2020). *J. Environ. Chem. Eng.* **8**, 103666.
2. C. Chen, W. Ma, and J. Zhao (2010). *Chem. Soc. Rev.* **39**, 4206.
3. N. Sobana, M. Muruganadham, and M. Swaminathan (2006). *J. Mol. Catal. A: Chem.* **258**, 124.
4. L. Leontie, M. Caraman, M. Alexe, and C. Harnagea (2002). *Surf. Sci.* **507–510**, 480.
5. W. Li (2006). *Mater. Chem. Phys.* **99**, 174.

6. G. Bandoli, D. Barecca, E. Brescacin, G. A. Rizzi, and E. Tondello (1996). *Chem. Vap. Depos.* **2**, 238.
7. H. Woo Kim (2008). *Thin Solid Films* **516**, 3665.
8. M. Schuisky and A. Harsta (1996). *Chem. Vap. Depos.* **2**, 235.
9. P. M. V. Almeida, C. B. Gozzo, E. H. N. S. Thaines, A. J. M. Sales, R. G. Freitas, A. J. Terezo, A. S. B. Sombra, and M. M. Costa (2017). *Mater. Chem. Phys.* **10**, 1.
10. J. Deng and Z. Zhao (2018). *Comput. Mater. Sci.* **142**, 312.
11. S. Schmidt, E. T. Kubaski, D. P. Volanti, T. Sequinel, V. D. N. Bezzon, and S. M. Tebcherani (2018). *Part Sci. Technol.* https://doi.org/10.1080/02726351.2018.1457108.
12. N. Sugimoto, H. Kanbara, S. Fujiwara, K. Tanaka, and Y. Shimizugawa (1999). *J. Opt. Soc. Am. B* **16**, 1904.
13. M. Drache, P. Roussel, and J.-P. Wignacourt (2007). *Chem. Rev.* **107**, 80–96.
14. J. Yu and A. Kudo (2006). *Adv. Funct. Mater.* **16**, 2163.
15. H. Cheng, B. Huang, J. Lu, Z. Wang, B. Xu, X. Qin, X. Zhang, and Y. Dai (2010). *Phys. Chem. Chem. Phys.* **12**, 15468.
16. Z. Ai, Y. Huang, S. Lee, and L. Zhanga (2011). *J. Alloys. Compd.* **509**, 2044.
17. A. Hameed, T. Montini, V. Gombac, and P. Fornasiero (2008). *J. Am. Chem. Soc.* **130**, 9658.
18. Z. Bian, J. Zhu, S. Wang, Y. Cao, X. Qian, and H. Li (2008). *J. Phys. Chem. C* **112**, 6258.
19. H. Y. Jiang, J. Liu, K. Cheng, W. Sun, and J. Lin (2013). *J. Phys. Chem. C* **117**, 20029.
20. S. Anandan, G. Lee, P. Chen, C. Fan, and J. J. Wu (2010). *Ind. Eng. Chem. Res.* **49**, 9729.
21. V. Bekiari, M. Sotiropoulou, G. Bokias, and P. Lianos (2008). *Colloid Surf. A* **312**, 214.
22. M. Mallahi, A. Shokuhfar, M. R. Vaezi, A. Esmaeilirad, and V. Mazinani (2014). *Am. J. Eng. Res.* **3**, 162.
23. A. K. Hezama, Q. A. Namrathaa, Z. H. Drmoshb, Q. A. Yamanib, and K. Byrapaa (2017). *Ceram. Int.* **43**, 1.
24. K. Vasanth- Kumar, K. Porkodi, and F. Roch (2008). *Catal. Commun.* **9**, 82.
25. C. G. Da Silva and J. L. Faria (2003). *J. Photochem. Photobiol. A* **155**, 133.
26. N. Serpone and A. Emeline (2002). *IJP* **2**, 91.
27. M. Movahedi, A. R. Mahjoub, and S. Janitabar-Darzi (2009). *JICS* **6**, 570.
28. R. S. Dariani, A. Esmaeili, A. Mortezaali, and S. Dehghanpour (2016). *Optik* **12**, 7143.
29. J. Hong, N. Ta, S. Yang, Y. Liu, and C. Sun (2007). *Desalination* **214**, 62.
30. T. Saison, N. Chemin, C. Chaneac, O. Durupthy, V. Ruaux, L. Mariey, F. Mauge, P. Beaunier, and J. P. Jolivet (2011). *J. Phys. Chem. C* **115**, 5657.
31. I.K. Konstantinou and T.A. Albanis (2004). *Appl. Catal. B*: 491.
32. T. N. Soitah, Y. Chunhui, Y. Yong, N. Yinghua, and S. Liang (2010). *Appl. Phys.* **10**, 1372.
33. N. M. Mahmoodi, M. Arami, N. Y. Limaee, and N. S. Tabrizi (2006). *J. Colloid Interface Sci.* **295**, 159.
34. Y. C. Wu, Y. C. Chaing, C. Y. Huang, S. F. Wang, and H. Y. Yang (2013). *Dyes Pigm.* **98**, 25.
35. M. Jalalah, M. Faisal, H. Bouzid, J. G. Park, S. A. Al-Sayari, and A. A. Ismail (2015). *J. Ind. Eng. Chem.* **30**, 183.
36. L. Song and S. Zhang (2010). *React. Kinet. Mech. Catal.* **99**, 235.
37. W. Raza, A. Khan, U. Alam, M. Muneer, and D. Bahnemann (2016). *J. Mol. Struct.* **1107**, 39.
38. S. M. Yakout (2020). *J. Environ. Chem. Eng.* **8**, 103644.

Publisher's Note